

CHAPTER 4

AEROSOL HYGROSCOPICITY

The hygroscopic nature of fine aerosols (particles $<2.5 \mu\text{m}$) was examined by the NPS group of researchers during SEAVS. The aerosol size distribution and light scattering coefficient were measured at relative humidities ranging from $<15\%$ RH to $>90\%$ RH. The scattering coefficient was measured as a function of RH using a Radiance Research M903 nephelometer, while the aerosol size distribution was measured as a function of RH with a Particle Measuring Systems ASASP-X optical particle counter. The humidity of the sample aerosol for both instruments was controlled using Perma Pure Nafion drying tubes mounted in a “constant” temperature inlet. This system was operated such that alternating “dry” (RH $<15\%$) then “wet” (RH $>20\%$) measurements of aerosol size distributions and scattering coefficients were made.

Varying the RH of the purge air used in the Perma Pure drying tubes controlled the RH of the aerosol sample. Purge air RH was varied by increasing or decreasing the voltages to mass flow controllers that regulated the flow of dry and saturated purge air streams. By appropriately mixing the flow of dry and saturated purge air streams, any sample RH between $<15\%$ and $>90\%$ could readily be achieved. The voltages to the mass flow controllers were controlled either manually with a potentiometer or automatically with a programmed Campbell 21X data logger. Sample RH was controlled manually when both the optical particle counter (OPC) and the nephelometer were operated simultaneously. Manual control was used during OPC operation because this instrument required longer sampling periods at a single RH value. Automated RH control was used when the nephelometer alone was sampling. The sample RH and temperature were continuously monitored inside the sampling plenum (a schematic diagram is shown in Figure 2.9), at the outlet of the optical particle counter (immediately downstream of the optical cavity), and at the outlet of the nephelometer (a few inches downstream from the optical chamber). The instruments and inlet used in this experiment were described more thoroughly in Chapter 2.

4.1 AEROSOL SIZE DISTRIBUTION MEASUREMENTS AS A FUNCTION OF RH

Time lines of daily averaged “dry” (RH $<15\%$) aerosol size distribution parameters, including number concentration, volume, mass mean diameter, and geometric standard deviation derived from OPC data are shown. The time lines of “dry” aerosol data illustrate how the particle-size distribution varied during SEAVS. The “dry” data also serves as a check on the reasonableness of assumptions made for data inversions. The aerosol water uptake is reported, as D/D_o where D is the geometric mean diameter of particles at a given RH value and D_o is the geometric mean “dry” particle diameter. Finally, the measured water uptake of the ambient aerosol is compared to theoretical calculations of water uptake for a pure ammonium bisulfate aerosol.

4.1.1 Characterization of “Dry” Aerosol Size Distributions

The OPC data, obtained during measurement of “dry” aerosol, was inverted by correcting for the difference in refractive index of the polystyrene latex spheres, which were used for calibrations, and the refractive index of the “dry” aerosol. The refractive index of the “dry” aerosol was estimated using partial molar refractive indices [Stelson, 1990] and chemical composition data from the IMPROVE sampler. In these calculations, the accumulation mode aerosol (generally particles $<1.0 \mu\text{m}$) is assumed to be internally mixed and composed of sulfate, ammonium ion, and carbon (both elemental and organic). The mass of soil (i.e., elements: Si, Al, and Fe) was ignored in these calculations because only accumulation mode aerosols were considered when estimating the volume distribution parameters of the dry aerosol. This rationale is justified by the presence of a larger mode in the size distribution when the aerosol was composed of a significant fraction ($>20\%$) of soil elements. It is assumed these larger particles are composed primarily of soil elements. The refractive index of the “dry” aerosol, estimated on a daily basis, is shown in Figure 4.1. During SEAVS, the calculated refractive index ranged from 1.47 to 1.53; the mean value was 1.51. In processing the “dry” size distribution data, an index of refraction of 1.52-0i was used for Julian days (JD) 195 through 221 and 1.50-0i for JD 222 through 233.

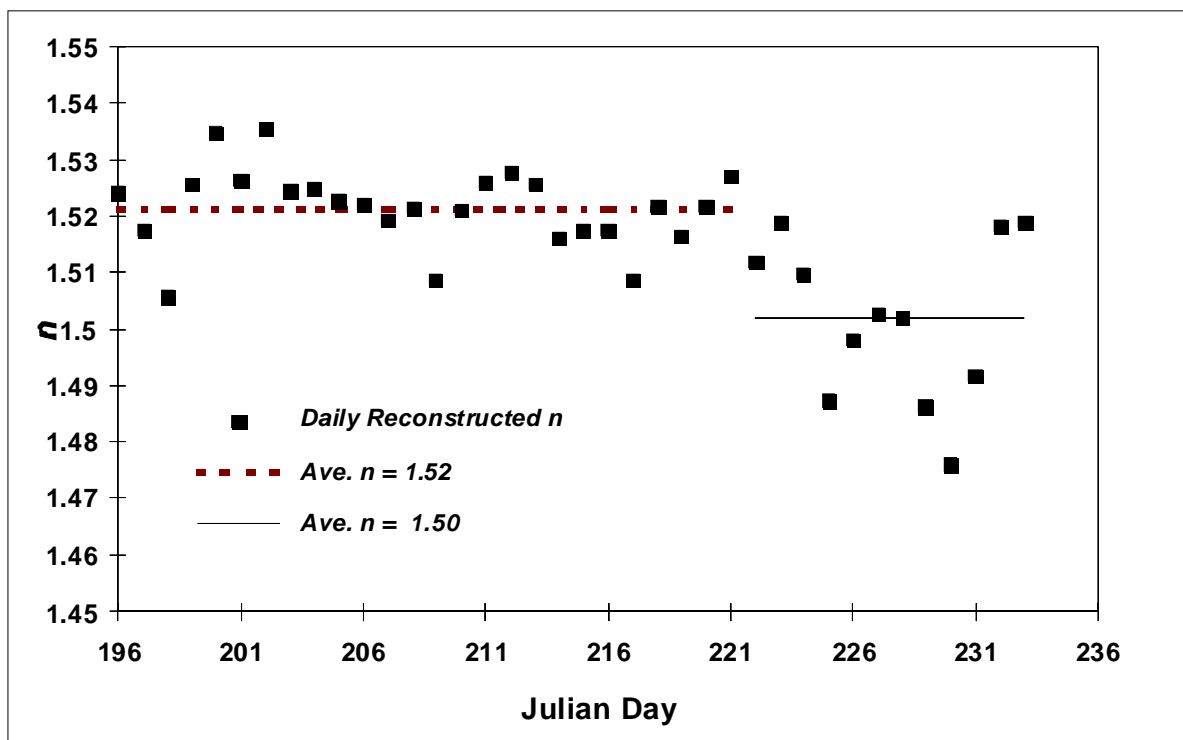


Figure 4.1 Dry aerosol refractive index, n , reconstructed using chemical data from the IMPROVE sampler. The two average refractive index values used to process OPC data are highlighted with solid and dashed lines.

A time line of daily averaged “dry” aerosol number concentration, obtained by integrating aerosol number concentration over the size range from $0.1 < \text{particle diameter } (D_p) < 2.5 \mu\text{m}$, is

presented in Figure 4.2. Daily averages of the volume distribution parameters, which include volume concentration ($\mu\text{m}^3 \text{cm}^{-3}$), mass mean diameter (MMD, μm), and geometric standard deviation (σ_g) are also displayed in Figure 4.2. The volume distribution parameters represent accumulation mode aerosol, typically in the $0.1 < D_p < 1.0 \mu\text{m}$ size range, however, the upper limit of the size range was adjusted with a floating cutoff point. The size distribution parameters were calculated using statistical formulas given in Knutson and Liou [1982]. Time periods characterized by similar meteorological conditions [Sherman *et al.*, 1996] are superimposed on this figure to illustrate how they bracket the temporal increase and decrease in the aerosol number concentration for the accumulation mode aerosol. The dry aerosol volume distribution parameter statistics calculated over the entire study period are given in Table 4.1.

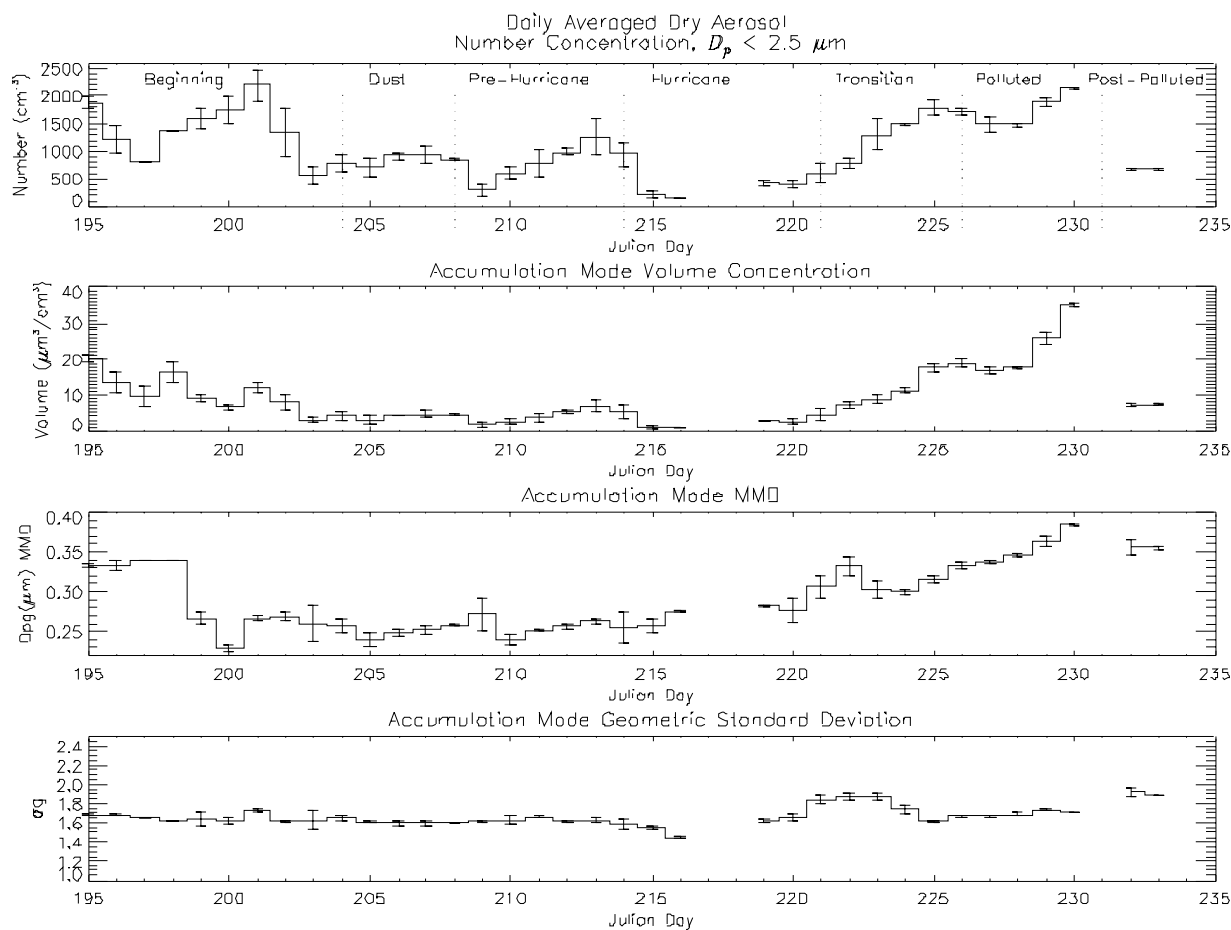


Figure 4.2 Dry aerosol size distribution parameter time lines. The first plot shows aerosol number concentration integrated over particle diameters from 0.1 to 2.5 μm . The lower three plots are volume distribution parameter time lines for accumulation mode aerosol. Time periods of similar meteorological conditions are superimposed on the number concentration time line to show the relationship between meteorological conditions and aerosol number concentration.

Table 4.1 Summary statistics of “dry” aerosol distribution parameters.

Median Volume ($\mu\text{m}^3 \text{cm}^{-1}$)	Max.	Min.	Median MMD μm	Max.	Min.	Median σ_g
6.1	34.9	1.14	0.279	0.383	0.239	1.640

4.1.2 Dry Aerosol Volume and Density

The daily averaged aerosol volume concentrations from the OPC are compared to the aerosol mass concentrations from the IMPROVE sampler to determine consistency between the two data sets. Figure 4.3 shows time lines of aerosol mass concentration from the IMPROVE sampler and aerosol volume concentration from the OPC. The fine mass (particles $<2.5 \mu\text{m}$ in diameter) shown in Figure 4.3 is the sum of sulfate, ammonium ion, total carbon (elemental plus organic), and soil elements. Figure 4.3 shows the aerosol volume concentration and aerosol mass concentration exhibit similar temporal trends throughout the study.

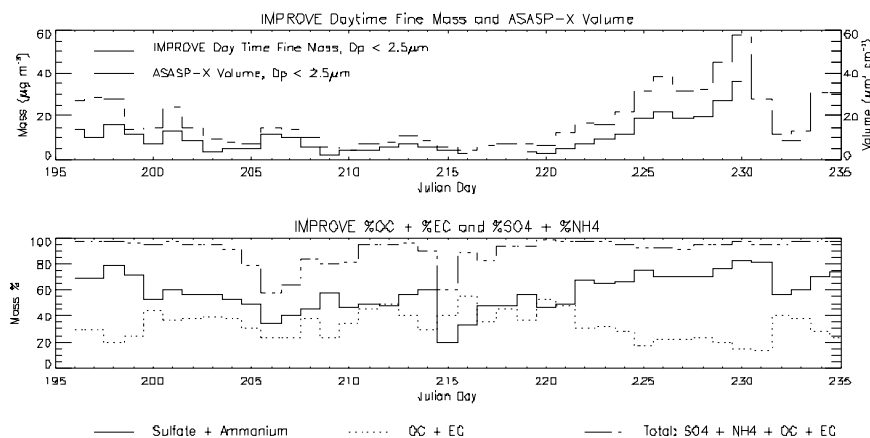


Figure 4.3 Time lines of aerosol volume concentration from the ASASP-X with aerosol fine mass from the IMPROVE sampler. Below is a time line for fine chemical mass expressed as a percent of sulfate plus ammonium, organic plus elemental carbon, and soil.

The lower plot in Figure 4.3 shows time lines of percent mass for: (1) (sulfate plus ammonium ion mass)/(total fine mass), (2) (carbon mass)/(total fine mass), and (3) (sulfate + ammonium ion + carbon)/(total fine mass). The total mass is defined as the sum of sulfate, ammonium ion, carbon, and soil elements. The predominance of sulfates and carbon is evident from Figure 4.3, with sulfate and its associated ammonium ion mass contributing to 50% or more of the fine aerosol mass on all but eight days.

The volume concentrations, shown in Figure 4.3, are not expected to include significant contributions from water, as the RH during sampling was less than 15%, however, some unknown quantity of water is almost certainly present on or within the sampled particles. Assuming water contributes little to the measured volume concentration under low (<15% RH) sampling conditions, the dry density of the aerosol can be estimated by taking the ratio of the mass and the volume concentrations. Figure 4.4 shows a scatter plot of 12-hour daytime mass concentrations obtained from the IMPROVE sampler versus volume concentration obtained from the OPC. The least squares regression line that was forced through zero gives an average density of 1.65 g cm^{-3} the median value was 1.67 g cm^{-3} . There is some scatter about the regression line, which is expected because of the chemical composition of the aerosol varied considerably during the study as shown in Figure 4.3. Some estimates of dry solute densities are listed in Table 4.2 for comparison to the experimentally derived aerosol densities. The internally mixed aerosol densities were computed assuming volume conservation of the respective pure phases. The densities calculated for mixtures of organic carbon and sulfate compounds represent the mass fraction range observed for these compounds during SEAVS. Since the OPC data used in this analysis is for $D_p < 2.5 \text{ }\mu\text{m}$, soil mass, with densities that may be greater than compounds used to calculate density in Table 4.2, may contribute to the aerosol density derived by experiment. However, the soil mass was generally small and therefore was expected to contribute little to aerosol dry density and has been neglected in these calculations.

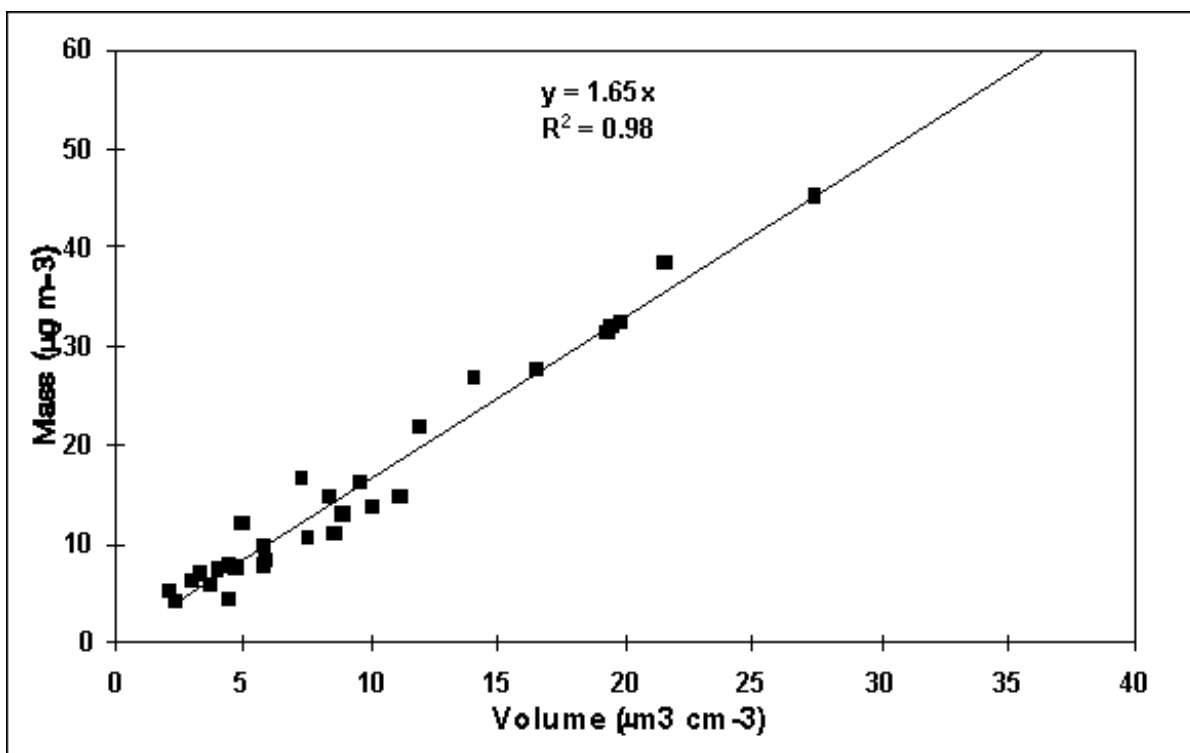


Figure 4.4 A scatter plot of dry aerosol fine mass concentration from the IMPROVE sampler and dry aerosol volume from the ASASP-X. A least squares regression of these data has a slope approximately equivalent to the median aerosol density, calculated as the mass to volume ratio for a given day.

Table 4.2 Comparison of dry density.

Compound	Density (g cm ⁻³)	Reference
Measured “Dry” Aerosol	1.67	$n = 1.520, 1.501$
Ammonium Sulfate	1.769	a
Ammonium Bisulfate	1.780	a
Sulfuric Acid (98%)	1.841	a
Organic Carbon	1.40	b
85% Ammonium Bisulfate, 15% Organic (by mass)	1.67	c
60% Ammonium Sulfate, 40% Organic (by mass)	1.63	c

n = Refractive indices to process dry aerosol distributions

^aCRC, 46th edition

^bStelson [1990]

^cCalculated by volume conservation

The quantities derived from OPC data, such as the “dry” density, depend upon the refractive index used to invert the data. The reconstructed “dry” refractive indices, shown in Figure 4.1, suggest appropriate values for inverting dry distribution data, however, to simplify data processing only two refractive index values were applied when the dry OPC data was inverted. A value of 1.52-0i was used from JD196 through JD 221 and a value of 1.501 was used from JD 222 through 232. Table 4.3 illustrates the “dry” density’s dependence on the refractive index used during data inversion. Median values and the standard deviations of calculated aerosol density are shown for: (1) the entire study period, (2) a time period of low aerosol concentration, and (3) a time period of high aerosol concentration using various indices of refraction to invert the OPC data. The median density for the entire study period calculated using an inversion refractive index of 1.53 was 1.87 g cm⁻³. This value of density is 14% greater than the value of density calculated using an inversion refractive index of 1.50. Since the aerosol parameters calculated from OPC data show a significant dependence on the refractive index used for inverting the OPC data, using a refractive index that reflects the changing aerosol composition should give more accurate results. However, the two indices of refraction used for inverting these data give reasonable results and will suffice as a first approximation.

4.1.3 Aerosol Water Uptake

In processing OPC data taken under humidified conditions, the dependence of the refractive index on water associated with the aerosol must be accounted for. Refractive index values were taken from published values [Shettle and Fenn, 1979] for a rural aerosol with similar composition to that of the aerosol measured in this study. The RH dependent refractive indices range from 1.53-

σ_i for dry conditions to 1.42-0i for RH >85%. These values are considered first approximations to actual values, and water uptake results herein can be revised with more accurate refractive index values if they become available.

Table 4.3 Comparison of density from different refractive indices.

Refractive Index	Median ρ_T g cm ⁻³	σ	Median ρ_L g cm ⁻³	σ	Median ρ_H g cm ⁻³	σ
1.520, 1.501	1.67	0.337	1.65	0.420	1.65	0.215
1.53	1.87	0.385	1.69	0.441	2.00	0.264
1.520	1.81	0.363	1.65	0.420	1.91	0.251
1.501	1.61	0.303	1.53	0.356	1.65	0.215

Figure 4.5 is an example of sequential dry and humidified aerosol size distributions measured by the OPC on JD 207. The first column of plots in this figure is the aerosol number distributions and the second column in the same row is the volume distributions. Moving from top to bottom in this figure portrays a series of sequential dry-humidified-dry distributions. The initial dry distribution is superimposed on the subsequent plots as a dotted line to indicate size shifts due to associated water. An obvious large aerosol mode is present in the volume distribution plots. This large mode is probably composed primarily of soil elements as data from the IMPROVE sampler indicates soil elements compose approximately 40% of the fine aerosol mass for this time period.

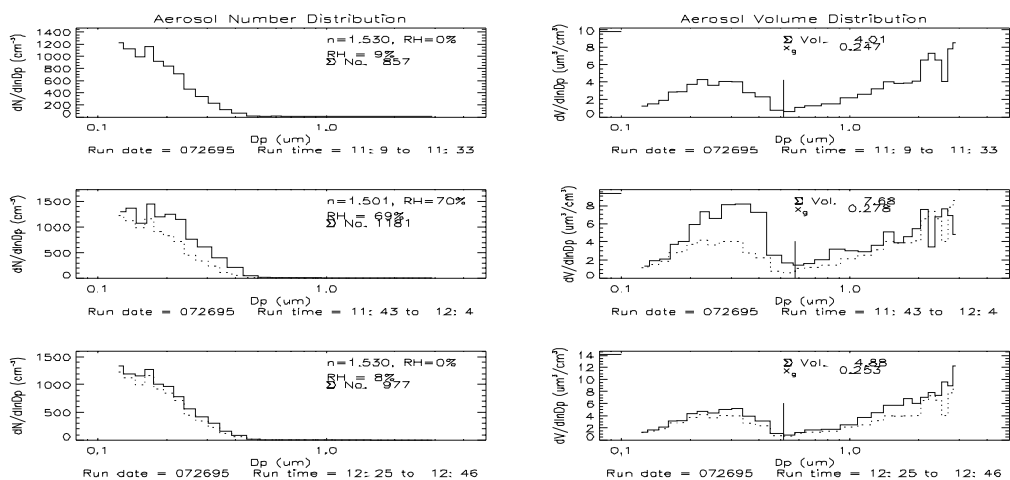


Figure 4.5 Sequential dry-humidified-dry aerosol distributions obtained on Julian day 207. The presence of a large aerosol mode corresponds to a high concentration of crustal elements observed in data from the IMPROVE sampler. The number distribution plots show the OPC data inversion refractive index (n), the RH that the inversion n applies

to, the experimental RH and total number concentration. Volume distribution plots show total volume concentration and MMD for the accumulation mode; the accumulation mode is demarcated by particle sizes less than the vertical solid line.

4.1.4 Derived Wet-to-Dry Aerosol Diameter Ratios

Particle size change as a function of RH can be expressed as a ratio of wet-to-dry particle diameter,

$$\frac{D}{D_o} = \left(\frac{V}{V_o} \right)^{\frac{1}{3}} \quad (4.1)$$

where D is the particle diameter at a given RH, D_o is the dry particle diameter, V is the wet integrated volume, and V_o is the dry integrated volume. The values of V and V_o are calculated from sequential dry then wet OPC measurements, which require approximately twenty minutes each to complete. Hereinafter the ratio D/D_o is referred to simply as R . Alternatively, R can be expressed as the volume geometric mean diameter, $D_{p,g}$ (MMD), ratio of humidified and dry aerosol volume distributions, provided the water uptake across the aerosol size distribution is homogeneous

$$\frac{D}{D_o} = \frac{D_{p,g}(Wet)}{D_{p,g}(Dry)} \quad (4.2)$$

McMurry [1996] reported size classified particles measured during SEAVS exhibited similar hygroscopic growth characteristics for particles with diameters between 0.1 and 0.4 μm , suggesting particle hygroscopicity across the aerosol accumulation mode is homogeneous.

Generally, R calculated by Equation (4.1) for the accumulation mode aerosol, and R calculated by Equation (4.2) for the entire OPC size range is consistent. However, during time periods when a significantly large aerosol mode is present, R calculated for the accumulation mode aerosol typically exceeded R calculated by including the large mode aerosol into the integrated volumes used in Equation (4.1). This apparent preferential water uptake by the accumulation mode aerosol may reflect preferential aerosol hygroscopicity, and therefore differences in aerosol chemical composition between the accumulation and large mode aerosol particles. Figure 4.6 shows value of R , calculated by the MMD ratio method (Equation 4.2). The dotted line is a polynomial best fit to the data.

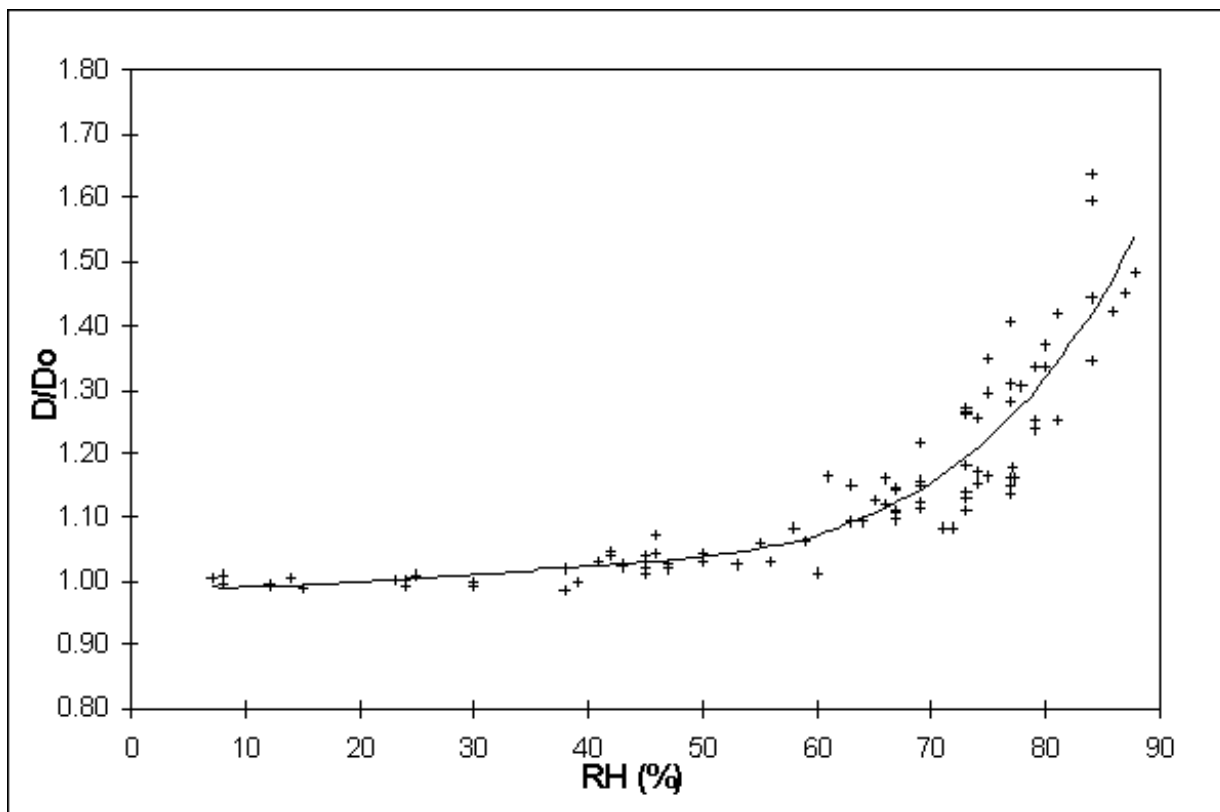


Figure 4.6 *RH dependent aerosol size change observed during SEAVS. D/D_0 values were calculated as the wet-to-dry aerosol distribution MMD ratio. The line is a polynomial best fit to the data.*

4.1.5 Comparison of Measured Water Uptake to Theoretical Water Uptake

Aerosol water uptake derived from experimental measurements is compared to estimated aerosol water uptake based on chemical mass fractions determined from IMPROVE sampler data. Aerosol hygroscopicity is estimated by adding water to the ionic mass according to empirical formulas that express pure solute water uptake. The mixing rule of Malm and Kreidenweis [1996] is used to estimate aerosol hygroscopicity from the chemical mass fractions. Sulfate, ammonium, organics, and elemental carbon are assumed the only species in the accumulation mode and are assumed to be internally mixed. In the mixing equation, sulfate and ammonium ion mass are treated as the only hygroscopic fraction and are characterized as ammonium bisulfate with RH dependent water content, expressed as R , adopted from Tang and Munkelwitz, [1994]. The crystallization branch of the ammonium bisulfate growth curve was used to estimate water uptake. Representing water uptake with ammonium bisulfate is justified by the fact that the average ammonium to sulfate molar ratio during SEAVS was close to that of ammonium bisulfate.

Figure 4.7 suggests the estimated water uptake by ionic species overpredicts actual measured aerosol water uptake. For all values of R above 36% RH, the estimated water uptake is greater than the measured water uptake by an average of 11%. Since the theoretical estimates of R correspond to the crystallization branch of the growth curve, the assumption that all soluble aerosols have

deliquesced is inherent. This theoretical estimate of aerosol hygroscopicity for the ionic fraction represents an upper limit in R provided particle acidity does not exceed that of ammonium bisulfate. If only some fraction of the particles in the size distribution have deliquesced at a given RH, for example, estimates of R would overpredict water uptake at a given RH.

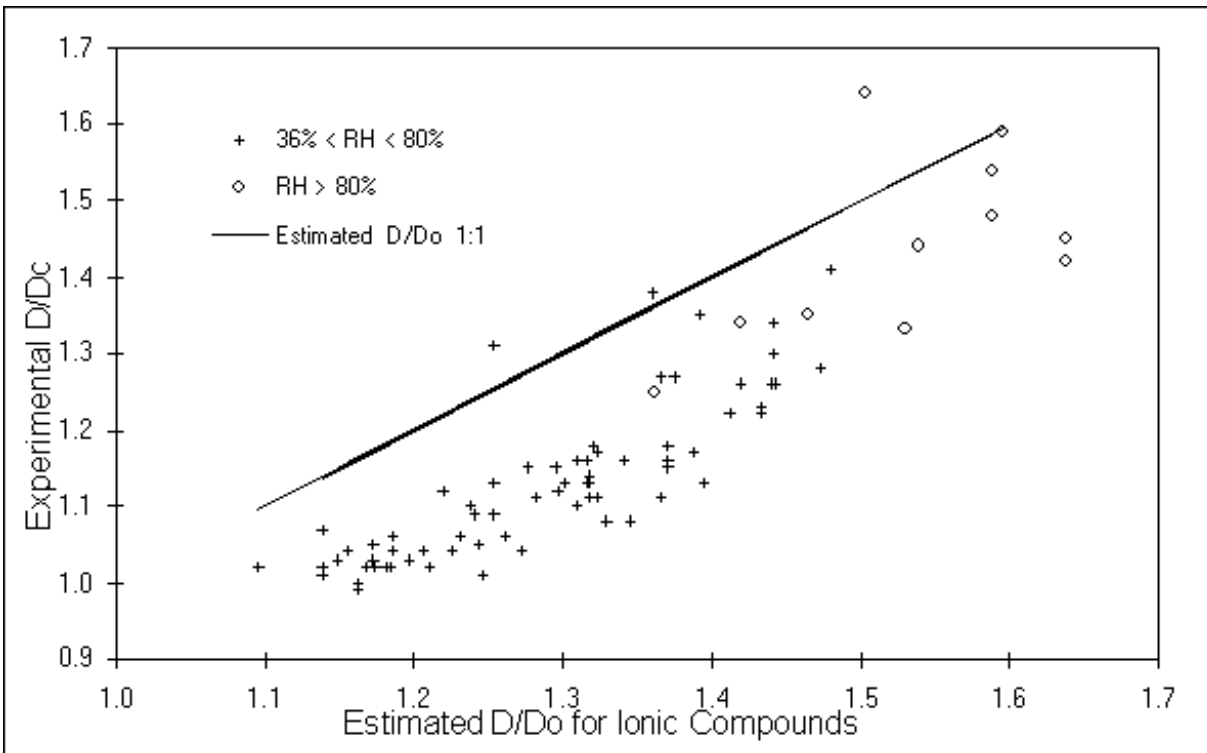


Figure 4.7 A scatter plot of experimentally determined D/D_o measured during SEAVS and theoretical estimates of D/D_o for daily averages of the ionic aerosol species. Experimental D/D_o is calculated as the wet-to-dry aerosol volume MMD ratio.

A more reliable comparison is to see if the experimental R values above 80% RH are significantly different than the estimated water uptake. Above 80% RH, all sulfate and most organics that exhibit deliquescence should have associated water and estimated water uptake should be comparable to experimental values. With this criterion applied, estimated water uptake over predicts experimental water uptake by 6%. The uncertainty in the experimentally derived data is at least 6%; therefore, these experimental data cannot be concluded to be significantly different than the estimates of water uptake for ionic species alone.

A shortcoming of the experimentally derived R estimates is the lack of detailed chemical information for accumulation mode aerosol. If some fraction of this aerosol mass is soil, or other insoluble species, then the estimated water uptake would decrease in an amount proportional to the mass of the insoluble material.

4.2 AEROSOL LIGHT SCATTERING MEASUREMENTS AS A FUNCTION OF RH

In this section, sample temperature and RH measurements and corrections to sample RH are discussed to establish the uncertainty in the RH measurement. Time lines of measurements are shown and the protocol for data reduction is given; this establishes the uncertainty in the scattering coefficient as a function of RH data set. Results of the measurements are presented and compared to various aerosol chemical compositions. Finally, the scattering coefficient measured as a function of RH is compared to that predicted from a simple model calculation.

4.2.1 Aerosol RH and Temperature Measurements

The aerosol sample's relative humidity was of fundamental importance to this experiment. The aerosol sample's RH and temperature were measured at the plenum, before entering the nephelometer, (see Figure 2.9) and at the outlet of the nephelometer. Because humidity is strongly affected by relatively small changes in temperature, an attempt was made to keep the entire sampling train at the same temperature. Keeping the temperature constant as the aerosol sample passes from the plenum and through the nephelometer will thereby keep the sample RH constant. To achieve this goal, an inlet was constructed that maintained the sample aerosol at a nearly constant temperature; the aerosol temperature, measured at the plenum, generally varied by less than 4°C per day and the average temperature throughout the study was 26.5°C .

The sample inlet, used during the study, consisted of 23 Perma Pure drying tubes mounted in parallel and housed in an insulated aluminum cylinder that was filled with water. The water bath temperature and subsequently the aerosol sample's temperature varied much less than the ambient temperature and the changes in aerosol sample temperature occurred much more slowly than the ambient temperature changes. During the study, the temperature of the aerosol sample inside the plenum was monitored and the temperature of the instrument enclosure, which housed the nephelometer and the optical particle counters, was maintained very close to the temperature of the plenum. Since the aerosol sample's temperature changed little throughout the day and because the temperature changes occurred slowly, the instrument enclosure could be maintained close to the temperature of the inlet with little effort. The temperature of the instrument enclosure was regulated manually by observing the plenum and instrument enclosure temperatures, which were displayed in real time on a computer screen, and then adjusting the temperature in the instrument enclosure using a reostated incandescent light to warm the enclosure or by porting cool air from inside the air conditioned NPS trailer into the instrument enclosure to lower its temperature. Air inside the instrument enclosure was continuously circulated using two small fans.

In general, the instrument enclosure temperature differed from the plenum temperature by less than 1°C. Figure 4.8 shows a typical time line of ambient, plenum, and instrument enclosure temperatures. The maximum temperature difference between the plenum and the instrument enclosure for Julian day 219, shown in Figure 4.8, was 0.74°C. For most of the day, the temperatures were less than 0.5°C different. The time periods when the temperatures drifted apart usually occurred during calibration of the OPC when the doors to the instrument enclosure were open. Temperature differences also occurred after prolonged OPC operation because the OPC's

power supply generated considerable heat. Since “dry” scattering measurements were often being made during the OPC calibrations, the temperature differences that occurred during OPC calibrations seldom had a significant impact on the relative humidity of the sample aerosol in the nephelometer.

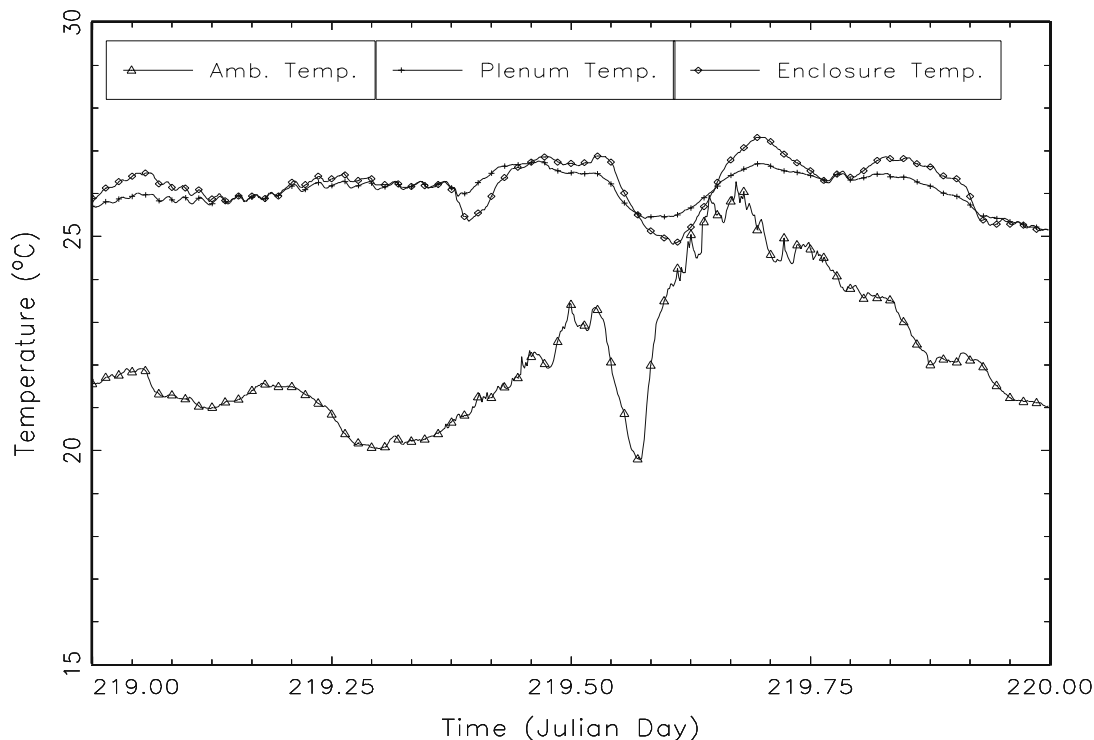


Figure 4.8 Comparison of ambient, plenum, and instrument enclosure temperatures. Showing the small temperature changes of the plenum, relative to ambient temperature changes, and the small difference in temperature between the plenum and the instrument enclosure.

There were time periods, however, when the temperature measured in the plenum (water bath temperature) was significantly different ($>2^{\circ}\text{C}$) from the temperature of the instrument enclosure. During these time periods there was often a correspondingly large difference between the RH measured at the plenum and the RH measured at the outlet of the nephelometer. The large difference between the RH measured at the plenum, before entering the nephelometer, and the RH measured at the outlet of the nephelometer leads to unacceptable uncertainty in the RH of the sample inside the nephelometer. Therefore, data collected during time periods when the plenum and instrument enclosure temperatures differed by more than 2°C and the RH differences exceeded 5% are not reported. Data, collected when the temperature difference between the plenum and outlet of the nephelometer was less than 2°C , were corrected for the expected change in RH that would occur for the measured change in temperature.

The temperature of the instrument enclosure, plenum temperature, plenum RH, and the analog b_{sp} signal from the nephelometer were recorded by a Campbell 21X data logger on two-minute averages. The temperature and RH of the sampled aerosol at the outlet of the nephelometer as well as the serial b_{sp} signal were logged by the nephelometer on five-minute averages. A comparison of

10-minute averaged data showed the instrument enclosure and outlet of the nephelometer were essentially in thermal equilibrium (nearly always $<0.5^{\circ}\text{C}$ difference). Since the temperature inside the instrument enclosure and the temperature at the outlet of the nephelometer agreed, and since it was advantageous to use the 2-minute averaged data set as opposed to the 5-minute averaged data set, the RH of the sample was corrected using the RH and temperature measured in the plenum and the temperature measured in the instrument enclosure. Figure 4.9 shows a typical comparison of the RH measured in the plenum and the RH calculated from the change in temperature between the plenum and nephelometer.

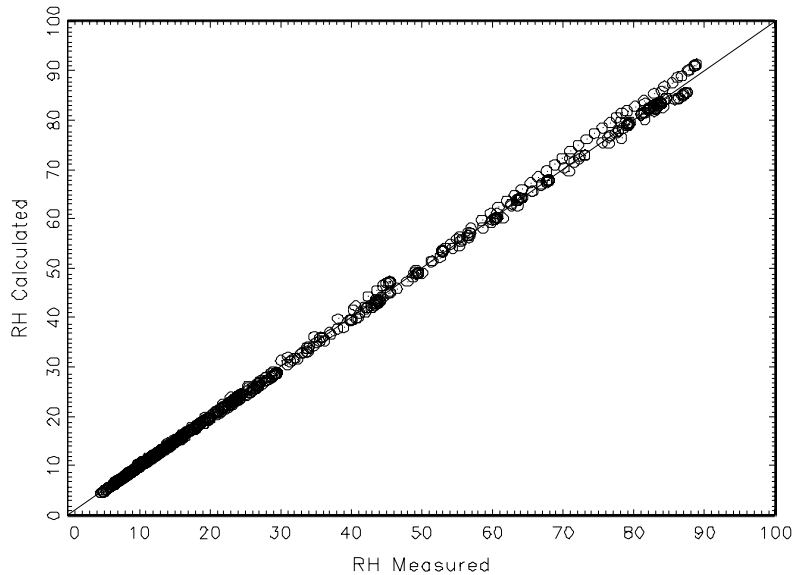


Figure 4.9 Scatter plot showing the typical difference between RH measured in the plenum and the RH corrected for the change in temperature between the plenum and the nephelometer.

The temperature inside the nephelometer's scattering chamber is unknown, however, it is assumed to be somewhere between the temperature measured at the plenum and the temperature measured at the outlet of the nephelometer. At higher RH values, the largest part of the uncertainty in the RH measurement is caused by the uncertainty in sample temperature. Since the instrument enclosure temperature and the outlet of the nephelometer were always within 0.5°C , an uncertainty in temperature of 0.5°C is assumed. The corrected RH values are reported graphically with error bars, which bound the possible RH values. The RH error bars are calculated using the temperature uncertainty of $\pm 0.5^{\circ}\text{C}$.

4.2.2 Aerosol Light Scattering Measurements

The scattering coefficient was measured while the RH of the aerosol sample was cycled from "dry" (RH $<15\%$) to humid (RH $>20\%$) and back to "dry" again. During automated RH control, each cycle required one hour to complete, however, during manual RH control the time between humid and dry measurements varied. Figure 4.10 shows a typical time line of the aerosol sample's

RH, represented as a fraction, and the scattering coefficient measured during automated RH control. Note that: (1) the RH of the sample is increased in increments of $\approx 20\%$ for each successive cycle, (2) there are at least three data points when the sample's RH is nearly constant ($<0.5\%$ RH difference between the data points) at the top of each cycle, and (3) there are, in general, several data points for $\text{RH} < 15\%$ at the beginning and at the end of each cycle. The three data points, obtained under humidified conditions when the sample's RH was nearly constant, were averaged to give one data point per cycle for sample RH and one data point per cycle for the scattering coefficient. The data points at the beginning of each cycle were averaged and the data points at the end of each cycle were averaged to give two "dry" scattering coefficient measurements for each cycle. Using this sampling procedure and this data acquisition criterion, one value of sample RH measured at an $\text{RH} \geq 20\%$, one value of the scattering coefficient corresponding to the RH value, and two "dry" scattering coefficient values are obtained for each RH cycle.

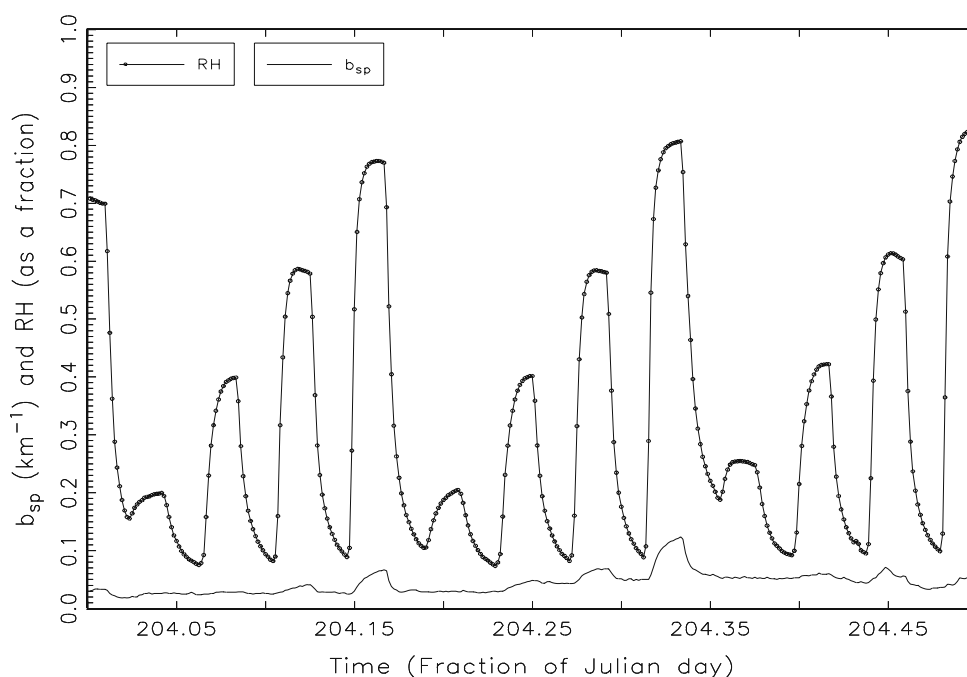


Figure 4.10 Time line showing the hourly RH cycle and subsequent change in scattering coefficient response to RH.

The ratio of b_{spw}/b_{spd} , where b_{spw} represents the scattering coefficient for some RH value $\geq 20\%$ and b_{spd} represents the "dry" scattering coefficient, is used to report the light scattering coefficient as a function of RH. The magnitude of the "dry" scattering coefficient, b_{spd} , measured at the beginning of a cycle, however, was sometimes considerably different than b_{spd} measured at the end of the same cycle. An example is shown in Figure 4.11. Note the dry scattering coefficient, emphasized by the first dashed line, is approximately 0.030 km^{-1} at 5:30 a.m. (204.25 as fraction of Julian day = 6:00 a.m.), however, one hour later the "dry" scattering coefficient, emphasized by the second dashed line, is approximately 0.044 km^{-1} . This represents about a 47% increase in the dry scattering coefficient over the duration of the RH cycle and leads to considerable uncertainty in the ratio b_{spw}/b_{spd} . However, if the increase in the scattering coefficient is relatively smooth and linear

over the time interval of the RH cycle, which was verified using b_{scat} values obtained from the ambient Optec nephelometers, then the mean of the “dry” measurements will be a reasonable estimation of the dry scattering coefficient at the time b_{spw} was measured. Therefore, the mean “dry” scattering coefficients, measured at the start and end of each cycle, were used to calculate the ratio. Furthermore, if the increase in the “dry” scattering for each RH cycle is relatively smooth and linear, the maximum value of the “dry” scattering coefficient will establish the minimum value for the ratio, while the minimum value of b_{spd} will establish the maximum value for the ratio. The data reported here uses the average value of b_{spd} to report the ratio and minimum and maximum values of b_{spd} to bound the ratio.

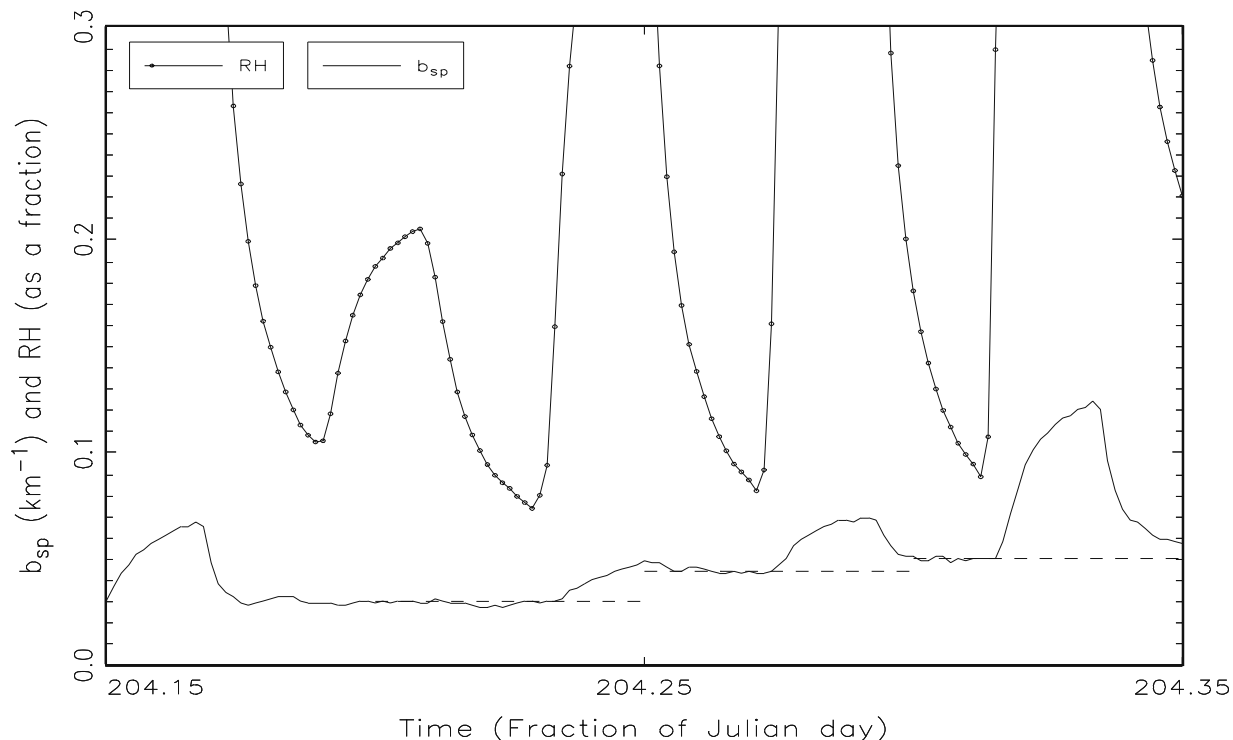


Figure 4.11 High resolution time line showing the change in “dry” scattering coefficient, which was often observed during an RH cycle. Large changes led to considerable uncertainty in the ratio used to report the change in scattering as a function of RH because the dry scattering was not known precisely when the humidified scattering was being measured.

4.2.3 Aerosol Light Scattering Data

The light scattering coefficient, measured as a function of RH and reported as the ratio of b_{spw}/b_{spd} , is shown in Figure 4.12. Note the scattering ratio, b_{spw}/b_{spd} , exhibits a smooth and continuous increase as the sample RH increases. No light scattering coefficient data, obtained during this study, exhibited an abrupt change as the aerosol’s humidity was either increased or decreased as would be expected if a large fraction of the aerosol particles were undergoing deliquescence or crystallization. This infers that at least a large fraction of ambient aerosol particles that were sampled during this study absorb water when the RH is increased and release water when RH is decreased in a smooth and continuous manner. Furthermore, since the scattering coefficient

did not decrease abruptly under low RH conditions, which would be expected if a large fraction of the aerosol particles abruptly crystallized, it is possible the aerosol particles were never completely dried to the point of crystallization.

Figure 4.12 also shows there are large variations in the magnitude of the ratio over small ranges of RH and the error bars, which bound the ratio, often times do not overlap. This suggests the observed differences are probably real. The larger differences in the ratio primarily occurred over longer time periods (i.e., days) and the data suggests the larger differences in the ratio are related to aerosol chemical composition. Figure 4.13 shows the scattering ratio as a function of RH and the chemical composition of the bulk aerosol for three different time periods during SEAVS. Note that the soluble inorganic fraction, which is composed primarily of sulfate, SO_4^{2-} , and ammonium ion, NH_4^+ , with smaller contributions to the soluble inorganic mass fraction from NO_3^- , Na^+ , and Cl^- , dominates the aerosol fine mass on Julian day 224 and the scattering ratio is considerably higher than either day 207 or day 211, which are dominated by soil and organic compounds, respectively.

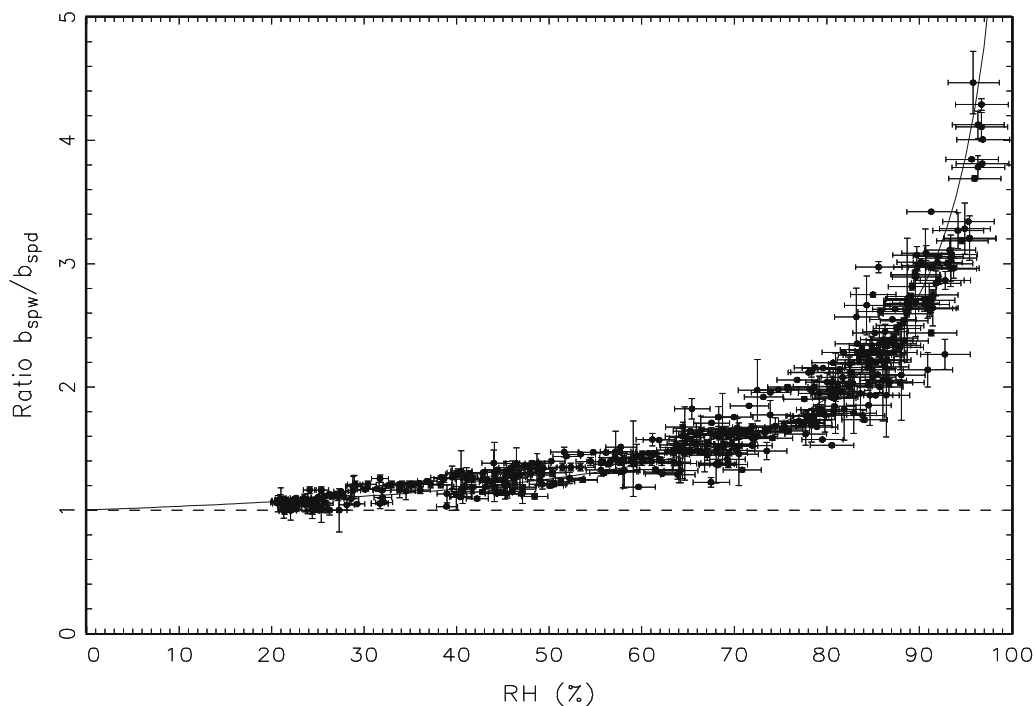


Figure 4.12 Plot showing the ratio of humidified scattering coefficient over “dry” scattering coefficient versus sample RH for all valid data obtained during SEAVS.

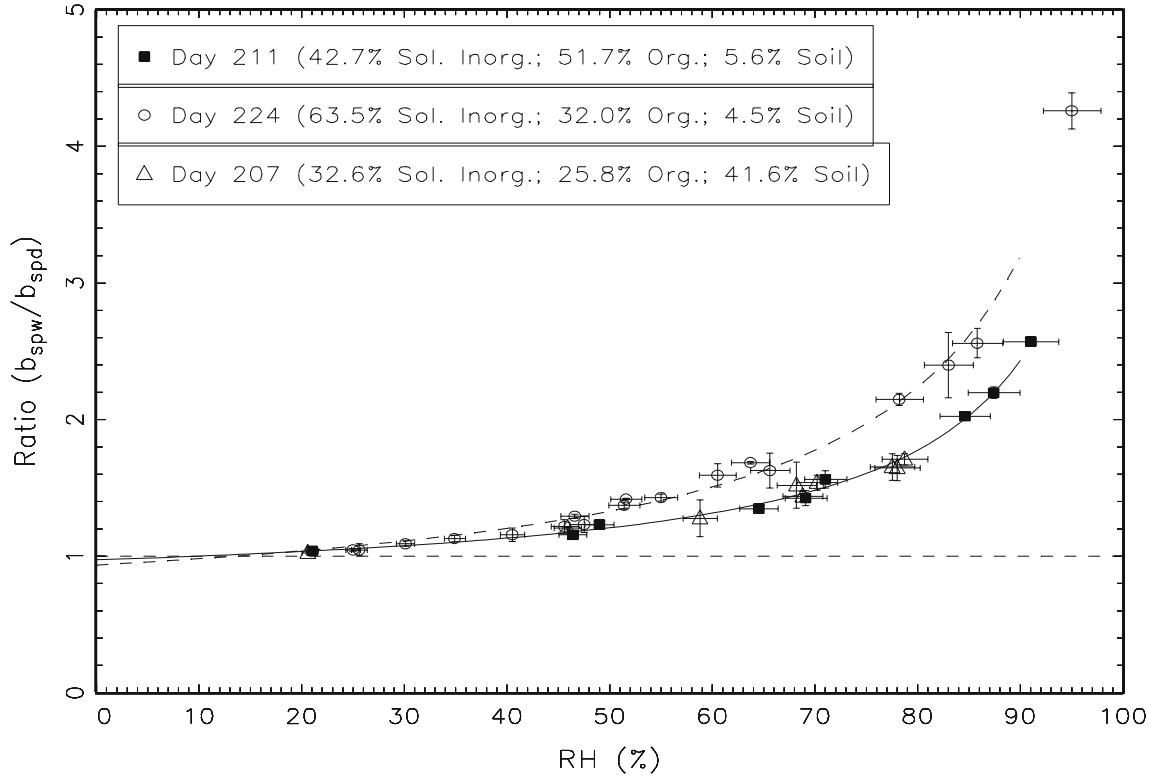


Figure 4.13 Plot showing the significantly different light scattering coefficient ratios that were observed for different aerosol compositions during SEAVS.

4.2.4 Comparison of Measured Scattering Ratio to Model Calculations

The scattering ratio, b_{spw}/b_{spd} , is compared here to a simple aerosol scattering model that utilizes aerosol mass, size distribution data for sulfate, and empirical aerosol growth curves to estimate the scattering coefficient. The equation used for estimating the scattering coefficient was:

$$b_{sp} = (eff_{sul})[sulfate](f(RH)) + 3[nitrate](f(RH)) + 4[organic] + 1[soil] \quad (4.3)$$

where (eff_{sul}) is the mass scattering efficiency for sulfate, which was calculated from the sulfate size distribution and Mie theory; the values 3, 4, and 1 are the assumed mass scattering efficiencies, which have units of $m^2 g^{-1}$, for nitrate, organic carbon, and soil, respectively; the term inside the brackets is the mass of the species measured by the IMPROVE sampler; and $f(RH)$ is an empirical growth function. The development of this model is fully discussed in sections 5.4.1 and 5.4.2.

To compare the measured scattering ratio to the scattering ratio obtained from the model calculations, Equation (4.3) is first computed without the growth term, $f(RH)$, which is associated with sulfate and nitrate only, to calculate the dry scattering coefficient. This produces an average dry scattering coefficient for the 12-hour IMPROVE sampler measurement period. Then Equation

(4.3) is recalculated using the $f(RH)$ term, which produces the scattering coefficient as a function of RH. Dividing the scattering coefficient values by the dry scattering coefficient value gives the model's scattering ratio as a function of RH, which can be compared directly to the scattering ratio measured as a function of RH.

Figures 4.14, 4.15, and 4.16 show the measured scattering ratio, indicated by the data points, and the modeled scattering ratio, indicated by the solid lines. Note that, in general, the modeled scattering ratio is slightly higher than the measured scattering ratio. This suggests the ambient aerosol may absorb slightly less water than is predicted from this model using empirical growth curves.

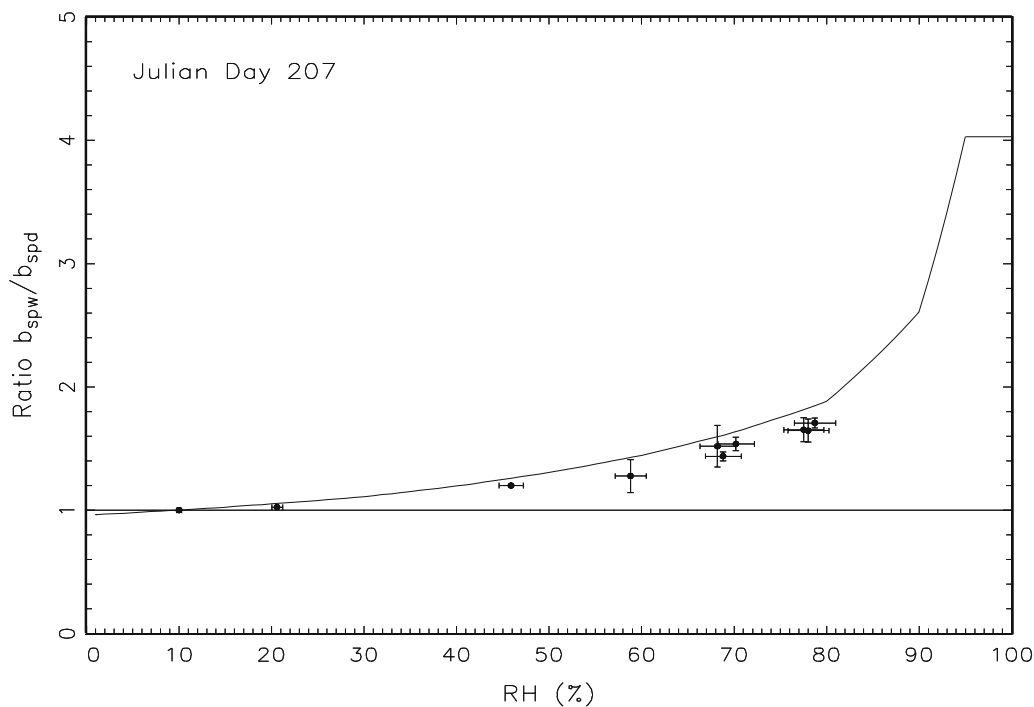


Figure 4.14 Comparison of measured scattering ratio and modeled scattering ratio versus RH.

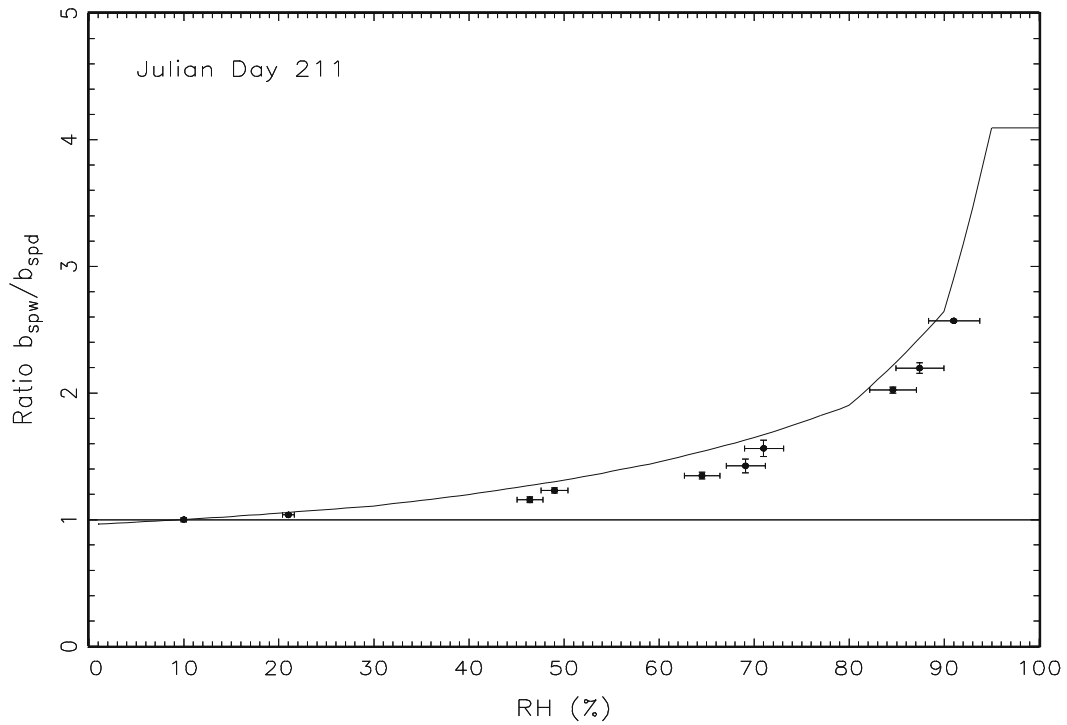


Figure 4.15 Comparison of measured scattering ratio and modeled scattering ratio versus RH.

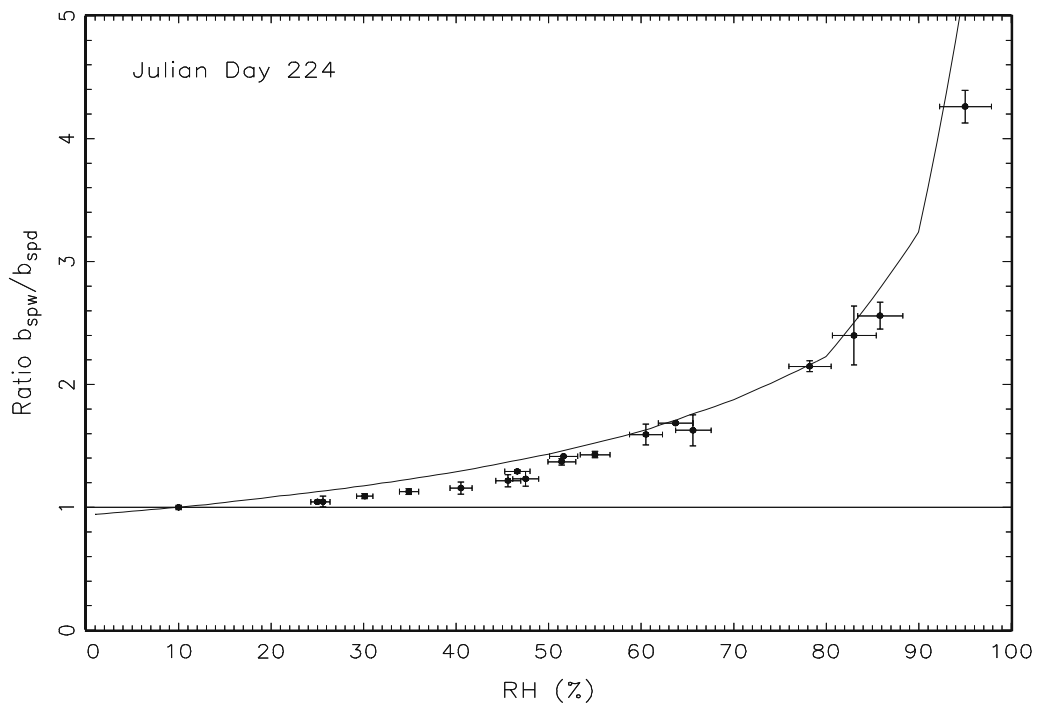


Figure 4.16 Comparison of measured scattering ratio and modeled scattering ratio versus RH.

4.3 REFERENCES

- Knutson, E.O. and P.J. Liroy, Measurement and presentation of aerosol size distributions, In air sampling instruments for evaluation of atmospheric contaminants, 7th edition, American Conference of Governmental and Industrial Hygienists, Cincinnati, Ohio, 1982.
- Malm, W.C. and S.M. Kreidenweis, The effects of aerosol hygroscopicity on the apportionment of extinction, submitted for publication in *Atmospheric Environment*, 1996.
- McMurry, P.H., Measurements of haze and visual effects, TDMA data report for the Southeastern Aerosol and Visibility Study, Electric Power Research Institute (EPRI), 1996.
- Sherman, D.E., R.B. Ames, and S.M. Kreidenweis, Influence of synoptic and local meteorological conditions on ambient total particle concentration during SEAVS, Paper No. 188, presented at the 13th ACS Rocky Mountain Regional Meeting, Denver Colorado, June 9-12, 1996.
- Shettle, E.P., and R.W. Fenn, Models for the Aerosols of the lower atmosphere and the effects of humidity variations on the optical properties, Environmental Research Paper, No. 676, AFGL-TR-79-0214, 1979.
- Stelson, A.W., Urban aerosol refractive index prediction by partial molar approach, *Environmental Science and Technology*, 24(11): 1676-1679, 1990.
- Tang, I.N., and H.R. Munkelwitz, Water activities, densities, and refractive indices of aqueous sulfates and sodium nitrate droplets of atmospheric importance, *Journal of Geophysical Research*, 99(D9): 18801-18808, 1994.